



Research Article

Design and analysis of dispersion-compensating chalcogenide photonic crystal fiber with high birefringence

S. James Raja¹ · S. Suriavel Rao² · R. Charlcedony²

Received: 11 June 2019 / Accepted: 19 February 2020 / Published online: 27 February 2020
© Springer Nature Switzerland AG 2020

Abstract

The photonic crystal fiber (PCF) with a bunch of air holes enclosing the silica core field has momentous and compelling attributes when compared with the ordinary single-mode fibers. In this work, both the birefringence and dispersion properties of a polarization-maintaining chalcogenide (ChG) photonic crystal fiber are numerically investigated by means of the finite element method. Through simulation, it is found that the birefringence of the proposed $\text{Ge}_{11.5}\text{As}_{24}\text{Se}_{64.5}$ PCF can reach as high as 0.03 when compared with the conventional fiber that has merely 5×10^{-4} for wavelengths in the 2–10 μm range. The PCF is designed with zero-dispersion wavelengths for x - and y -polarized modes in the 2–10 μm range. It is also observed that over the entire MIR wavelength range, the GVD remains positive and has a maximum value of 30,000 $\text{ps}^2/\text{nm}\cdot\text{km}$. Hence, the proposed $\text{Ge}_{11.5}\text{As}_{24}\text{Se}_{64.5}$ PCF plays the dual role of acting as a very good polarization-maintaining fiber due to its very high birefringence and an excellent dispersion-compensating fiber due to its large positive GVD. This $\text{Ge}_{11.5}\text{As}_{24}\text{Se}_{64.5}$ PCF serves as a very good candidate for ultra-broadband high bit-rate transmission. Supercontinuum generation is another important application of PCF. Supercontinuum generation is a generation of coherent and broadband light. SC generation in PCFs has several applications in optical coherence tomography (OCT), optical frequency metrology (OFM), pulse compression, and design of ultrafast femtosecond laser pulses.

Keywords Hexagonal lattice PCF · Single mode · Birefringence · Chromatic dispersion · Mid-IR wavelength · Nonlinear optics

1 Introduction

Photonic crystal fibers (PCFs) with the central defect region enveloped by multiple air holes that run along the fiber length have been captivating us and drawing our attention because of the unique features that cannot be accomplished in conventional fibers [1, 2]. PCFs possess exclusive and outstanding properties such as tailorable dispersion [3, 4], single-mode operation [5, 6], dispersion compensation, high birefringence [7, 8], large mode area [9, 10], and high nonlinearity, which are not achievable in ordinary silica fibers. Photonic crystal fibers offer a huge

diversity of features when compared to conventional fibers, which motivates us to develop advanced sensors with enhancement. These types of fibers have a few unique guiding features associated with the geometric aspects of the air holes and have been adopted in various systems. The birefringence and dispersion properties of the PCFs can be altered by changing the air-hole spacing (Λ), air-hole diameter (d), and the number of air-hole rings [11]. The symmetrical or non-symmetrical structure of PCF is attained by adjusting sizes, shape, or position of the air holes. The major factors contributing the limitations in conventional fibers are due to refractive index difference

✉ S. James Raja, jamesraja.tech@gmail.com | ¹Department of Electronics and Communication Engineering, National Institute of Technology Calicut, Calicut, Kerala, India. ²Department of Electronics and Communication Engineering, Karunya Institute of Technology and Sciences, Coimbatore, Tamil Nadu, India.



(Δ) of core and cladding. The lower values of Δ (for standard SMF, $\Delta \sim 0.4\%$) cause bending loss, and hence, the manipulation of group velocity dispersion (GVD) and birefringence is limited. The higher values of Δ (for MCVD, $\Delta \sim 10\%$) lead to increased attenuation due to absorption and Rayleigh scattering, and also, the single-mode core radius becomes very small. Another factor is the dependence on total internal reflection so that the propagation in a hollow core is unattainable [12]. PCFs have achieved finest performances in the applications of fiber sensors, fiber ring lasers, and nonlinear fiber optics. PCFs have been used in various fields based on their distinctive characteristics such as wavelength division multiplexing, great resilience, low transmission loss, high sensitivity, low manufacturing cost, and high efficiency.

One of the most fascinating properties of PCF is its high birefringence, which can be used for many practical applications such as fiber optic gyroscopes/hydrophones and polarization-maintaining erbium-doped fiber amplifiers/lasers. In order to get a large birefringence and to enhance the dispersion characteristics, elliptical air holes were employed in the cladding [13–15] or core area [16, 17]. From paper [18], it is found that the birefringence in the order of 10^{-2} has been achieved at $1.55 \mu\text{m}$ from their proposed structure made of solid silica core and a cladding with elliptical air holes. In paper [19], it is found that the birefringence in the order of 10^{-2} was achieved within wavelength range from 1.0 to $1.6 \mu\text{m}$ in the proposed rectangular lattice elliptical air-hole PCF. Paper [20] proposed squeezed lattice elliptical hole in both core and cladding and obtained a birefringence of about 0.065 . Paper [17] showed a birefringence of about 10^{-2} at $1.55 \mu\text{m}$ using a PCF made of circular air holes in cladding and rectangular array of four elliptical air holes in the core. In paper [21], birefringence of about 0.0025 was obtained at $1.55 \mu\text{m}$ from PCF with a central defect core and cladding with elliptical air holes. Moreover, in paper [22] a very high birefringence of about 4.8×10^{-2} was obtained by increasing the diameter of the two air holes adjacent to the central region. In addition, double circular-hole PCF, equiangular spiral PCF, rhombic-hole PCF, and rectangular-hole PCF were studied by [23–25], respectively. They obtained a maximum birefringence value of 0.01 , 0.0278 , 3.47×10^{-3} , and 1×10^{-3} , respectively. All these designs show an accelerated advancement in very high PCF design. However, practically speaking, it is not that simple to control the shape of the elliptical holes in the fabrication process. Also, all these fibers are based on traditional silica fiber material, which can be used only for wavelengths below $2 \mu\text{m}$, limited by material absorption. Today there has been a huge interest in the mid-infrared (MIR) spectral region ($2\text{--}20 \mu\text{m}$) [26] due to its various applications in biomedical imaging, coherence tomography, and

molecular spectroscopy [26–28]. Almost every molecule in this mid-infrared (MIR) region undergoes strong vibrational absorption. This provides possibilities for MIR spectroscopy to detect the quality of molecule category in a specific atmospheric condition [26, 29]. The mid-infrared (MIR) region contains two important spectral windows ($3\text{--}5 \mu\text{m}$ and $8\text{--}13 \mu\text{m}$), in which the atmosphere is translucent so that MIR spectroscopy can be used to smell out the scent of mysterious and toxic gases present in the atmosphere [26, 30]. Optical sources operated in the mid-infrared (MIR) region have many important applications in many areas such as gas sensing [31, 32] food quality control [31, 33], and medical diagnostics [31, 34]. Most of the photonic crystal fibers (PCFs) are fabricated using silica glass. Other glasses have also been used to achieve other particular optical properties. Silica is used because of its high refractive index. However, photonic crystal fiber made of silica glass only supports optical wavelengths in the visible and near-infrared regions because the material absorption is exceedingly large beyond $2 \mu\text{m}$ [31, 35]. To support optical wavelengths in the mid-IR region, several non-silica glasses have been recommended, including tellurite [31, 36, 37], fluoride [31, 38, 39], and chalcogenide (ChG) glasses [31, 40–43]. The fluoride and tellurite fibers support wavelength up to $5 \mu\text{m}$, whereas ChG fibers can be used over a wider window of up to $12 \mu\text{m}$ [31, 44]. Another important advantage is that ChG fibers possess very high optical nonlinearity, which is nearly thousand times greater than that of silica glasses [31]. This makes ChG glasses the most suitable host material in PCF fabrication than that of other materials, which could be used for several MIR region applications.

In this paper, we examined the birefringence and dispersion properties of a polarization-maintaining chalcogenide (ChG) photonic crystal fiber (PCF). The PCF is built of circular air hole, and it is a seven-ring hexagonal structure. The PCF is designed using an undoped silica material as well as the chalcogenide material to compare the performance of both the materials in different wavelength ranges. Undoped pure silica is used for applications in the near-IR region, whereas chalcogenide glass is used for applications in the mid-IR region wavelength region. Firstly, the geometrical parameters of PCF such as air holes, shape of air holes, number of air-hole rings, and the host material are chosen as per the requirement. The hole spacing, larger air-hole radius, and the smaller air-hole radius are fixed as $1.8 \mu\text{m}$, $0.8 \mu\text{m}$, and $0.6 \mu\text{m}$, respectively, in our paper. The effective indices of core modes in PCF are then calculated using the finite element method in COMSOL Multiphysics software. Once the effective index is determined as a function of wavelength, other parameters such as chromatic dispersion D , second-order dispersion β_2 , and birefringence B are calculated using well-known fiber

equations. The calculation and plotting of these parameters are done using MATLAB software. From calculations and plots, it is found that we got a very high birefringence of about 0.03 at 6.5 μm with ChG glass as a host material. Fiber with this high birefringence can be readily used as a high-performance polarization-maintaining fiber. Modern fiber optic communication systems are built with pulse widths as narrow as 10^{-12} s and with a data transmission rate going beyond 10^{12} bits/s. In a 15-Gb/s system, there are 15 billion bits per second. This trend of shrinking the pulse width and increasing the bit rate continues unflagging. The major problem we face while reducing the pulse width even further is the phenomena of pulse broadening due to different frequency components traveling at a different velocity. This phenomenon is called as GVD. To compensate the pulse broadening that occurred due to GVD, we are in need of dispersion-compensating fiber (DCF), which would nullify the effect of GVD. It is observed in our proposed design that we achieved a very high positive GVD of about 30,000 $\text{ps}^2/\text{nm.km}$. Fibers with positive GVD can act as DCFs, and hence, our proposed PCF can be a sure candidate to be used as a dispersion-compensating PCF for ultra-high-speed fiber optic data transmissions.

Supercontinuum generation is another important application of PCF. Supercontinuum generation is a generation of coherent and broadband light. This is due to the nonlinear interaction of laser pulse on nonlinear materials. The SC generation is due to the sequence of nonlinear processes such as self-phase modulation (SPM), self-steepening (SS), stimulated Raman scattering (SRS), and four-wave mixing (FWM). The advent of PCF has led to the revolution in generation of ultra-broadband spectra through SC generation. SC generation in PCFs has several applications in optical coherence tomography (OCT), optical frequency metrology (OFM), pulse compression, and design of ultra-fast femtosecond laser pulses [53].

2 Mathematical model

The numerical method used in this paper is the finite element method (FEM). The effective indices of core modes in PCF are evaluated using the finite element method. It is implemented in several optical waveguides to mathematically calculate chromatic dispersion, GVD, third-order dispersion coefficient, birefringence, and so on. Once the effective mode index n_{eff} is determined as a function of wavelength, the chromatic dispersion D can be calculated as:

$$D(\lambda) = -\frac{\lambda}{c} \frac{d^2 \text{Re}[n_{\text{eff}}]}{d\lambda^2} \quad (1)$$

Here, $\text{Re}[n_{\text{eff}}]$ is considered as the real part of the cladding effective index of PCF, c is the velocity of light in free space, and λ is the wavelength of operation. Chromatic dispersion is the combination of material and waveguide dispersion. Here, in our analysis, the material dispersion is assumed to be zero because its value is negligible when compared to the waveguide dispersion.

The second-order dispersion (β_2) is given by:

$$\beta_2 = -\frac{\lambda^2 D(\lambda)}{2\pi c} \quad (2)$$

where n denotes the effective index and λ denotes the wavelength of operation.

The third-order dispersion coefficient is mathematically found by this equation given below:

$$S = \left(\frac{2\pi c}{\lambda^2}\right)^2 \beta_3 + \left(\frac{4\pi c}{\lambda^3}\right) \beta_2 \quad (3)$$

where S indicates the slope of the dispersion coefficient D .

The difference between the two perpendicularly polarized effective indices is used to calculate the birefringence of PCF [24].

$$B = \left| \text{Re}(n_{\text{eff}}^x - n_{\text{eff}}^y) \right| \quad (4)$$

where B denotes the birefringence, $\text{Re}(n_{\text{eff}}^x - n_{\text{eff}}^y)$ is the real part of the effective index difference, and n_{eff}^x and n_{eff}^y are the refractive indices of the x - and y -polarized fundamental modes, respectively.

3 Methodology

Figure 1 shows the geometry of the advanced PCF design proposed in this paper. The PCF is built of circular air hole, and it is a seven-ring hexagonal structure [45]. The PCF is designed using an undoped silica material with a regular series of air holes passing across the surface of the cladding. The light is guided in the single mode along the central region of the fiber where one air hole is missing. The central region acts as a core.

The PCF in Fig. 1 resembles a hexagonal structure. The larger air holes are of radius $R = 0.8 \mu\text{m}$ and smaller air holes are of radius $r = 0.6 \mu\text{m}$. The hole spacing (pitch, Λ) is fixed as $1.8 \mu\text{m}$. We aim to optimize the design parameters so that the PCF exhibits a very high birefringence as well as all normal dispersion over a wide wavelength range. It is found that $r = 0.6 \mu\text{m}$, $R = 0.8 \mu\text{m}$, $\Lambda = 1.8 \mu\text{m}$ are the optimum values that yield most affirmative and favorable for the dispersion and birefringence. The air-filling ratio (D/Λ) is 0.888 in the central row of the fiber,

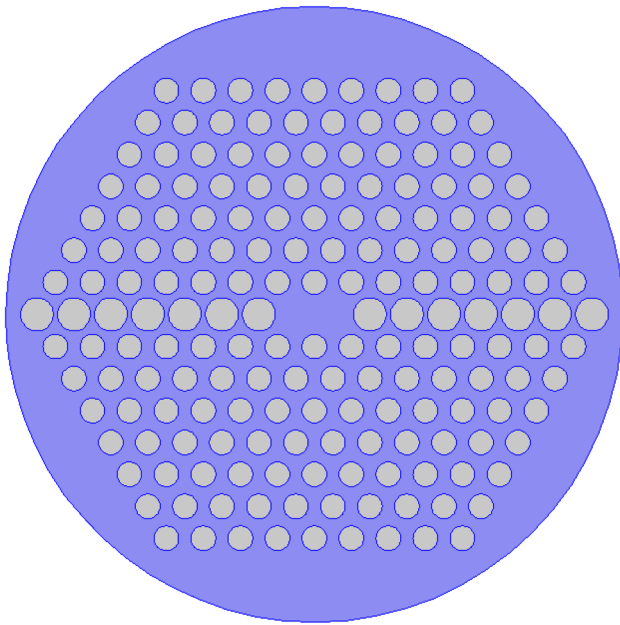


Fig. 1 Schematic representation of the proposed PCF

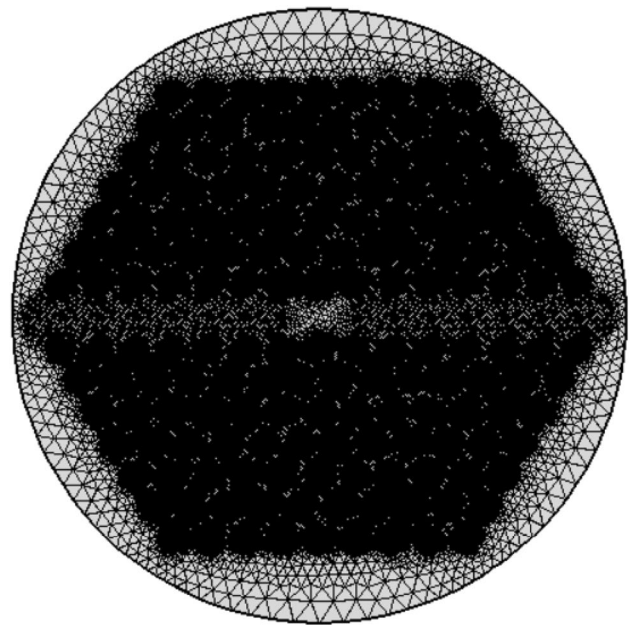


Fig. 2 Mesh of the proposed structure

and the ratio (d/Λ) is 0.666 for all other regions surrounding the core. The air-filling ratio is chosen to be large enough so that the mode field is confined in the central core region. Choosing larger air-filling ratio also introduces a good gap between air holes so that the air holes are not easily collapsed during fabrication [46].

The proposed PCF is endlessly single mode because it is an index-guiding PCF. The guiding property of the index-guiding PCF is qualitatively characterized by the air-filling fraction (d/Λ) . Strictly speaking, an index-guiding PCF does not need a clear boundary between the core and cladding regions. Light transmission in this kind of fibers is due to the index-difference effect.

The host material used is pure silica while working in the near-IR region, whereas chalcogenide glass is used for mid-IR region wavelengths. The ChG material is used so as to obtain a very high refractive index contrast between the core and the cladding, which results in a strong light confinement inside the core almost in all wavelengths [47]. Different characteristics of the proposed PCF are analyzed using the finite element method (FEM) with perfectly matched layer (PML) boundary conditions [48].

Choosing a right computational numerical technique for solving a problem is very important. If we choose a wrong technique, it can end up in incorrect result or it takes a very long time to compute the results. Transient response and impulse field effects are more accurately computed by using the finite difference time-domain (FDTD) method. Finite element method (FEM) is used for

accurate computations in curved geometrical objects. BEM is used for problems where Green's functions are to be calculated. They are usually used for computations in linear homogenous media.

The design of PCF is done by a step-by-step systematic procedure. In the first step, the important geometrical parameters of the PCF such as diameter of the air holes, shape of the air holes, number of air-hole rings, and the material are chosen as per the requirement. In the next step, the wavelength-dependent refractive index of the chalcogenide material is calculated and specified using the Sellmeier equation [54]. The Sellmeier equation is given by:

$$n_{\text{mat}}^2(\lambda) = 1 + \frac{5.78525\lambda^2}{\lambda^2 - 0.28975^2} + \frac{0.39705\lambda^2}{\lambda^2 - 30.39338^2} \quad (5)$$

This is followed by mesh generation. The meshing of the proposed structure is depicted in Fig. 2. By this mesh feature, the geometry model is characterized into small units called mesh elements. This is called discrete characterization. Every element in the mesh is controlled by a set of characteristic equations. These characteristic equations are partial differential equations (PDEs) that describe the physical properties of the material and the boundary conditions. These PDEs can be solved using analytical methods. Instead, these PDEs can be approximated with numerical model equations using discrete characterization and can be solved using numerical methods. Finite element method (FEM) is the numerical method, which

Fig. 3 Intensity distribution of fundamental modes: **a** x-polarized and **b** y-polarized

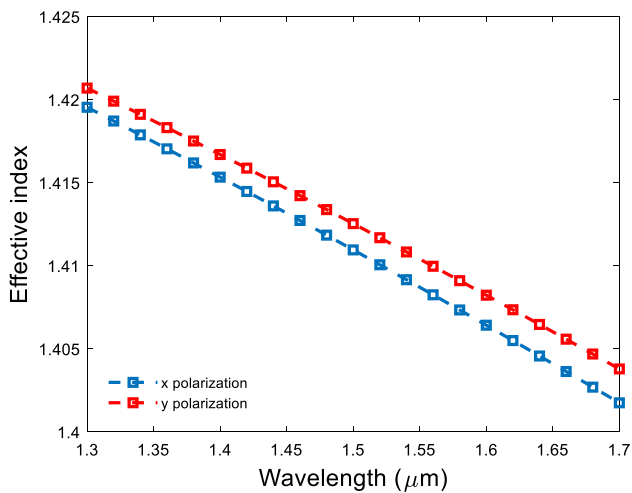
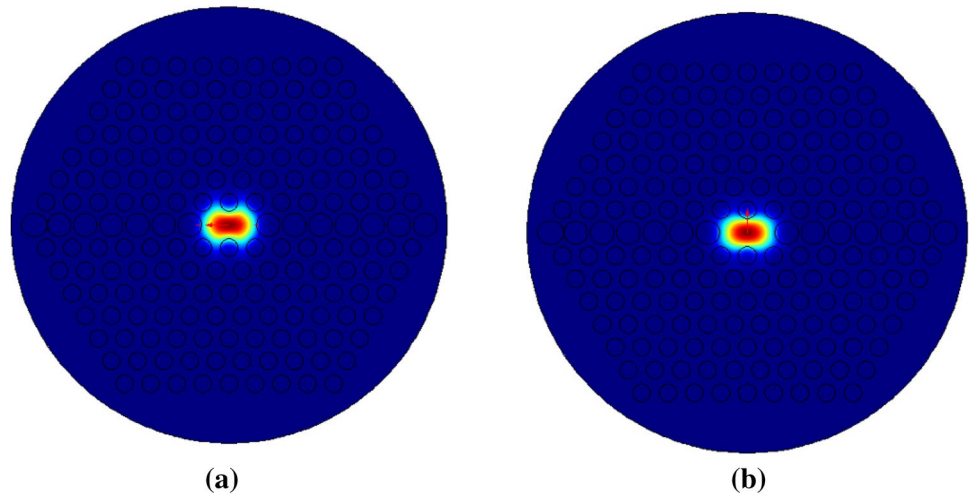


Fig. 4 Effective index curve of silica-glass PCF as a function of wavelength from 1.3 to 1.7 μm

is used to solve the PDEs so as to compute the effective index of the modes supported by the fiber. Finally, chromatic dispersion, GVD, and birefringence are calculated using the computed effective index.[49].

4 Results and discussion

4.1 Silica-glass PCF

The field intensity distribution of the guided modes are shown in Fig. 3. It is clearly seen in the figure that, at the central core region, the field distribution has its maximum intensity. Figure 4 shows the effective index as a function of wavelength from 1.3 to 1.7 μm, where the radius of larger air holes and smaller air holes is $R=0.8\ \mu\text{m}$ and $r=0.6\ \mu\text{m}$, respectively. We find a gradual decrease

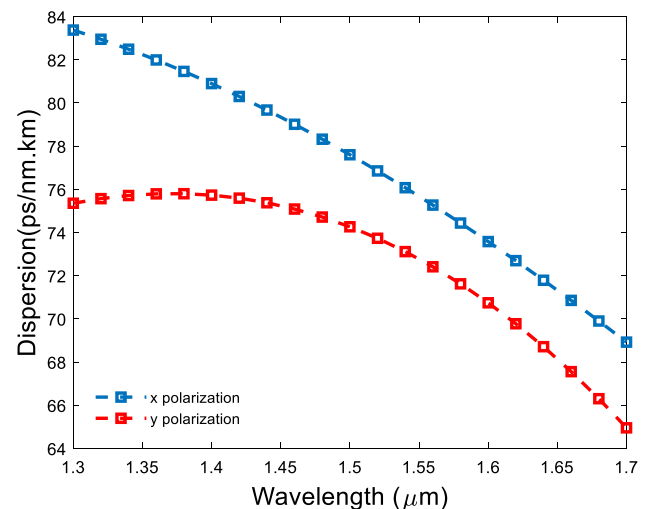


Fig. 5 Chromatic dispersion curve of silica-glass PCF

in the effective indexes of x-polarized and y-polarized modes with the increase in wavelength in the 1.3–1.7 μm range. It is worth noting that the y-polarized mode has a higher refractive index than that of the x-polarized mode throughout the wavelength range. All numerical calculations such as chromatic dispersion, GVD, and birefringence are performed with MATLAB.

The chromatic dispersion (D) is a mix of waveguide and material dispersion. It is a momentous and a pressing parameter of PCF, and it performs a significant and crucial role in fiber optic communication systems because it restricts the data-transmitting capacity of the optical fiber. Due to the effect of chromatic dispersion, the pulse at different wavelengths travels at different velocities inside the fiber. This finally results in pulse broadening. In PCF, the chromatic dispersion term can be engineered based on the conditions required for the practical applications. The

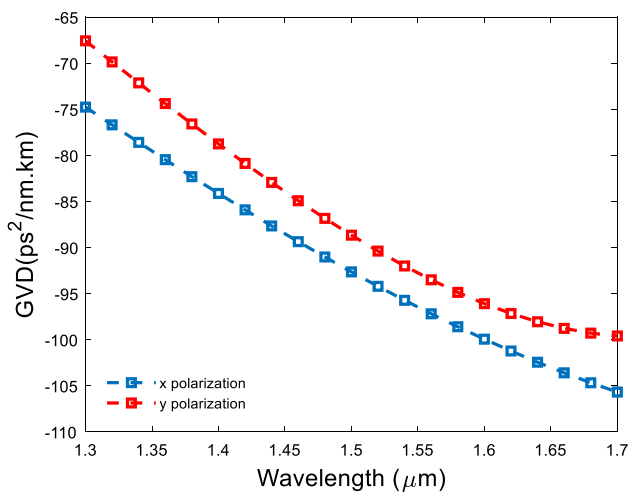


Fig. 6 Group velocity dispersion curve of silica-glass PCF

chromatic dispersion (D) and GVD (β_2) curves of the x - and y -polarized modes for the proposed PCF are depicted in Figs. 5 and 6, respectively. The chromatic dispersion (D) and GVD are calculated using Eqs. 1 and 2, respectively. It is seen in Fig. 5 that the chromatic dispersion gradually decreases with the increase in wavelength. The chromatic dispersion of the x -polarized mode is greater than that of the y -polarized mode in the entire wavelength range. In the calculated band, the dispersions appear to be positive. The y -polarized mode has a more smooth and linear variation in dispersion than that of the x -polarized mode. Also, it is clear from the graph that there is no zero-dispersion wavelength appearing for both x - and y -polarized modes in the wavelength range (1.2–1.7 μm). The dispersion of the PCF exhibits the maximum positive dispersion value of 83.4 ps/km/nm at a wavelength of 1.3 μm .

Figure 6 illustrates the GVD curve. From the curve, it is found that the GVD is inverse to the chromatic dispersion (D). The GVD decreases steadily with the increase in wavelength. In the calculated band, the dispersions appear to be negative, which means the fiber operates in the anomalous dispersion regime in this entire wavelength range (1.2–1.7 μm). Fibers with abnormal dispersion are very useful for building wavelength-tunable lasers and fiber ring lasers [50–52].

Figure 7 is the birefringence versus wavelength curve. The birefringence (B) is calculated using Eq. 4. It is observed that the birefringence constantly increases with the increase in wavelength. By removing air holes in the central part of the structure, an asymmetry is introduced in Fig. 1. It is a notable point that the birefringence is increased by reducing the larger and smaller air-hole gap and increasing the asymmetry of the configuration. We get the maximum value of 0.002 for birefringence at the

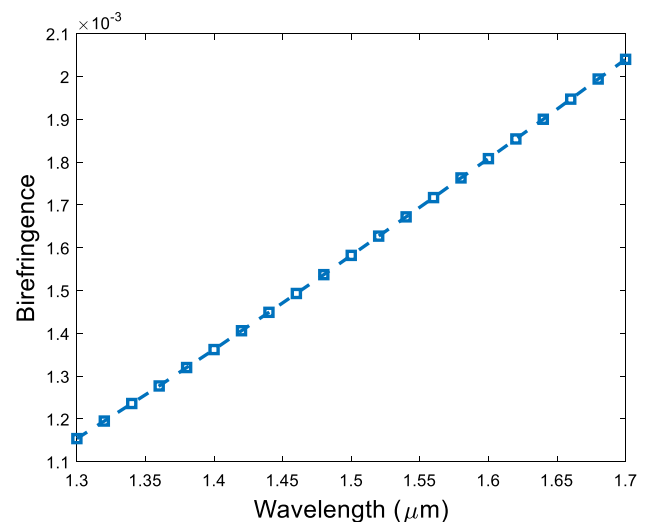


Fig. 7 Birefringence curve of silica-glass PCF

wavelength of 1.7 μm , which is many times greater than what is got from conventional polarization-maintaining fibers.

It is clearly seen in the figure that at the central core region the field distribution has its maximum intensity in case of both the x -polarized and y -polarized fundamental modes.

It is worth noting that the y -polarized mode has a higher refractive index than that of the x -polarized mode throughout the wavelength range.

It is observed that the chromatic dispersion of the x -polarized mode is greater than that of the y -polarized mode in the entire wavelength range. In the calculated band, the dispersions appear to be positive. The dispersion of the PCF exhibits the maximum positive dispersion value of 893.4 ps/km/nm at a wavelength of 1.3 μm .

Comparing Fig. 6 with Fig. 5, it is found that the GVD curve is inverse to the chromatic dispersion (D) curve. The GVD decreases steadily with the increase in wavelength. In the calculated band, the dispersions appear to be negative, which means that the fiber operates in the anomalous dispersion regime in this entire wavelength range (1.2–1.7 μm).

It is observed that the birefringence constantly increases with the increase in wavelength. We get the maximum value of 0.002 for birefringence at the wavelength of 1.7 μm , which is around 10 times greater than what is got from conventional polarization-maintaining fibers.

4.2 ChG-PCF

Figure 8 shows the effective index as a function of wavelength from 2 to 10 μm where the radius of larger air holes and smaller air holes are $R=0.8 \mu\text{m}$ and $r=0.6 \mu\text{m}$,

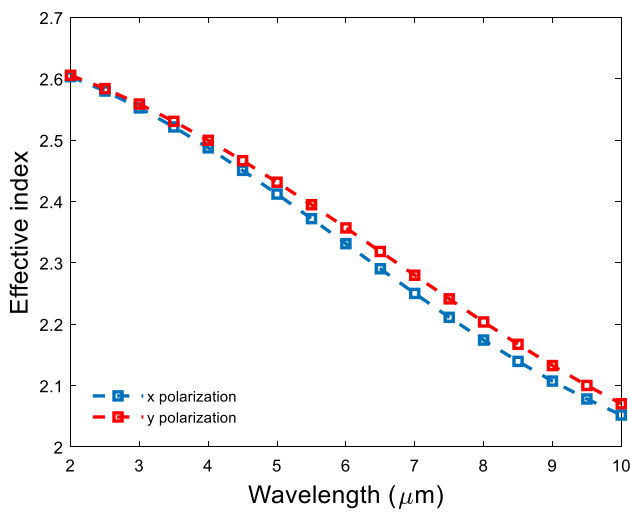


Fig. 8 Effective index curve of ChG-PCF as a function of λ between 2 and 10 μm

respectively. The effective index varies from 2.6 to 2.05 in this wavelength range. We find a gradual decrease in the effective indexes of x-polarized and y-polarized modes with the increase in wavelength in the 2–10 μm range. It is worth noting that the y-polarized mode has a higher refractive index than that of the x-polarized mode throughout the wavelength range. The numerical calculations such as chromatic dispersion, GVD, third-order dispersion, and birefringence are performed with MATLAB.

The chromatic dispersion (D) and GVD (β_2) curves of the x- and y-polarized modes for the proposed PCF are depicted in Figs. 9 and 10, respectively. The chromatic dispersion (D) and GVD are calculated using Eqs. 1 and 2, respectively. It is seen in Fig. 9 that the chromatic

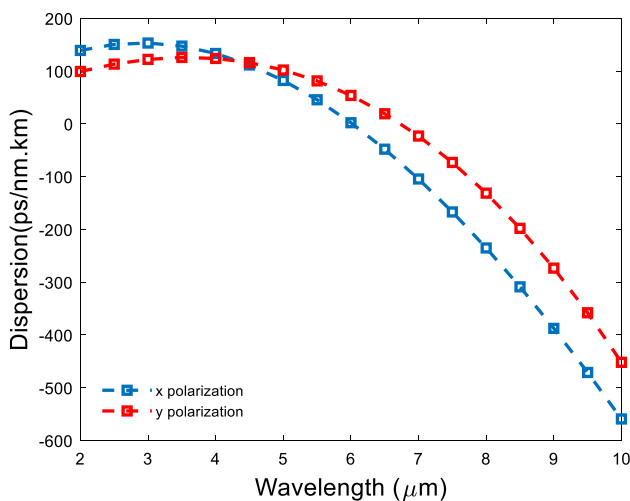


Fig. 9 Chromatic dispersion curve of ChG-PCF

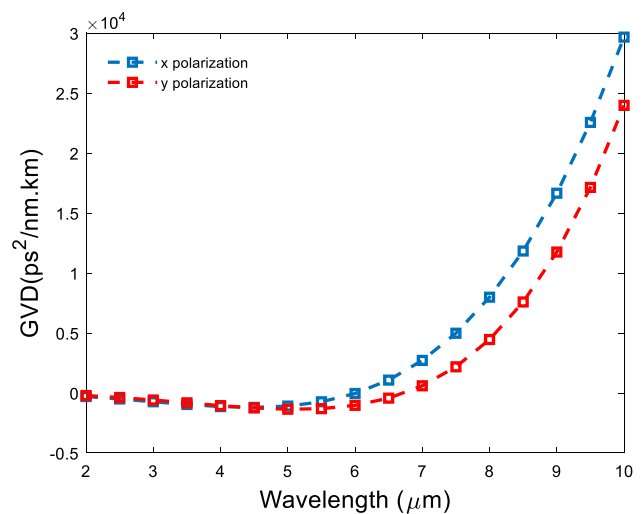


Fig. 10 Group velocity dispersion curve of ChG-PCF

dispersion gradually decreases with the increase in wavelength. The chromatic dispersion of the y-polarized mode is greater than that of the x-polarized mode almost in the entire wavelength range. In the calculated band, the dispersions appear to be positive for smaller wavelengths and negative for larger wavelengths. In the x-polarized mode, the dispersion becomes negative beyond 6 μm , and in the y-polarized mode, the dispersion becomes negative beyond 6.5 μm . Also, it is observed from the graph that there is zero-dispersion wavelength appearing for both x- and y-polarized modes in the wavelength range (2–10 μm). The dispersion of the PCF exhibits the maximum negative dispersion value of -560 ps/km/nm at a wavelength of 10 μm .

Figure 10 illustrates the GVD curve. From the curve, it is found that the GVD is inverse to the chromatic dispersion (D). The GVD increases steadily with the increase in wavelength. In the calculated band, the GVD appears to be negative for smaller wavelengths and positive for larger wavelengths. In the x-polarized mode, the dispersion becomes positive beyond 6 μm , and in the y-polarized mode, the dispersion becomes positive beyond 6.5 μm . The GVD takes the maximum value of 30,000 ps/nm.km at 10 μm . It is seen that the PCF exhibits a large positive value of β_2 . Fibers that possess a positive value of β_2 are called DCFs.

Figure 11 depicts the birefringence versus wavelength curve. The birefringence (B) is calculated using Eq. 4. It is observed that the birefringence constantly increases with the increase in wavelength up to 7.5 μm , and then, it starts gradually decreasing. We get a maximum value of 0.03 for birefringence at the wavelength of 6.5 μm , which is many times greater than what is got from conventional polarization-maintaining fibers.

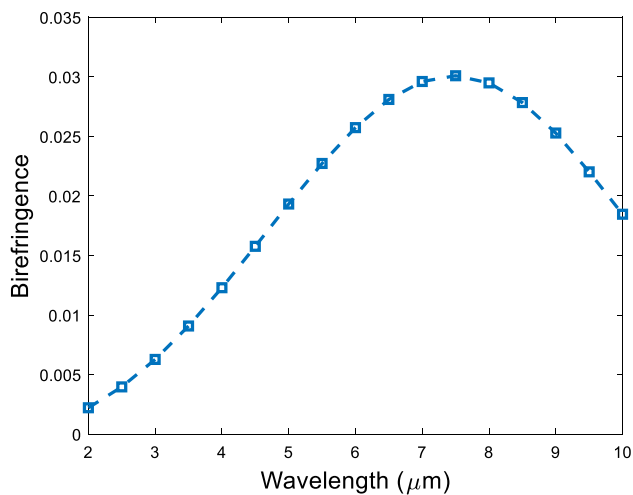


Fig. 11 Birefringence curve of ChG-PCF

We find a gradual decrease in the effective indexes of x -polarized and y -polarized modes with the increase in wavelength in the 2–10 μm range. The effective indexes decrease from 2.6 to 2.05 in this wavelength range. It is worth noting that the y -polarized mode has a higher refractive index than that of the x -polarized mode throughout the wavelength range.

It is seen in the figure that the chromatic dispersion gradually decreases with the increase in wavelength. The chromatic dispersion of the y -polarized mode is greater than that of the x -polarized mode almost in the entire wavelength range. In the calculated band, the dispersions appear to be positive for smaller wavelengths and negative for larger wavelengths. In the x -polarized mode, the dispersion becomes negative beyond 6 μm , and in the y -polarized mode, the dispersion becomes negative beyond 6.5 μm . Also, it is clear from the graph that there is zero-dispersion wavelength appearing for both x - and y -polarized modes in the wavelength range (2–10 μm). The dispersion of the PCF exhibits the maximum negative dispersion value of -560 ps/km/nm at a wavelength of 10 μm .

The GVD increases steadily with the increase in wavelength. In the calculated band, the GVD appears to be negative for smaller wavelengths and positive for larger wavelengths. In the x -polarized mode, the dispersion becomes positive beyond 6 μm , and in the y -polarized mode, the dispersion becomes positive beyond 6.5 μm . The GVD takes the maximum value of 30,000 ps/nm.km at 10 μm . It is seen that the PCF exhibits a large positive value of β_2 . Fibers that possess a positive value of β_2 are called DCFs.

It is observed that the birefringence constantly increases with the increase in wavelength up to 7.5 μm and beyond that it starts gradually decreasing. We get

a maximum value of 0.03 for birefringence at the wavelength of 6.5 μm , which is 100 times greater than what is got from conventional polarization-maintaining fibers.

5 Conclusion

PCFs have optical properties such as very high birefringence and large negative dispersion, which are almost unattainable in conventional fibers. A highly birefringent dispersion-compensating $\text{Ge}_{11.5}\text{As}_{24}\text{Se}_{64.5}$ PCF has been designed and studied. It is shown through the simulation results that the proposed PCF can provide a negative dispersion of about -560 ps/km/nm, at a wavelength of 10 μm . It is also found that, for the proposed ChG-PCF, the y -polarized fundamental mode possesses a higher chromatic dispersion than the x -polarization. The GVD is calculated for both the x - and y -polarized modes, and it is seen from the analysis that GVD reaches a maximum value of 30,000 ps²/nm-km at 10 μm . Hence, we can say that the PCF exhibits a larger positive value of β_2 . Fibers that possess a positive value of β_2 are called DCFs. Simulation results also show that a very high birefringence of about 0.03 can be obtained with $R=0.8$ μm and $r=0.6$ μm at the wavelength of 6.5 μm . In the investigation, it is found that by adjusting the smaller and larger air holes and varying the air-hole rings, the dispersion and birefringence can be precisely controlled. Hence, the fiber can be an assuring candidate for applications such as broadband dispersion compensation in optical communication systems and can be very well used as a polarization-sensitive device.

Compliance with ethical standards

Conflict of interest On behalf of all authors, the corresponding author states that there is no conflict of interest.

References

1. Broeng J, Mogilevstev D, Barkou SE, Bjarklev A (1999) Photonic crystal fibers: a new class of optical waveguides. *Opt Fiber Technol* 5:305–330
2. Birks TA, Knight JC, Mangan BJ, Russell PSJ (2001) Photonic crystal fibers: an endless variety. *IEICE Trans Commun* E84(C):585–592
3. Liu Y, Wang J (1999) A novel hybrid photonic crystal dispersion compensating fiber with multiple windows. *Opt Laser Technol* 44:2076–2079
4. Jer T, Shen LF, Chau YF (2008) High birefringence and low loss circular air-holes photonic crystal fiber using complex unit cells in cladding. *Opt Commun* 281:4334–4338

5. Knight JC, Birks TA, Russell PSJ, Atkinand DM (1996) All-silica single-mode optical fiber with photonic crystal cladding. *Opt Lett* 21:1547–1549
6. Knight JC, Birks TA, Cregan RF, de Sandr J-P (1998) Large mode area photonic crystal fibres. *Electron Lett* 34:1347–1348
7. Chen D, Shen LF (2007) Highly birefringent elliptical-hole photonic crystal fibers with double defect. *J Lightwave Technol* 25:2700–2705
8. Bhattacharya R, Konar S (2012) Extremely large birefringence and shifting of zero dispersion wavelength of photonic crystal fibers. *Opt Laser Technol* 44:2210–2216
9. Mortensen NA, Nielsen MD, Folkenberg JR, Petersson A, Simonsen HR (2009) Improved large-mode-area endlessly single-mode photonic crystal fibers. *Opt Lett* 28:393–395
10. Ademgil H, Haxha S (2012) Endlessly single mode photonic crystal fiber with improved effective mode area. *Opt Commun* 285:1514–1518
11. Maji PS, Chaudhuri PR (2016) Studies of the modal properties of circularly photonic crystal fiber (C-PCF) for high power applications. *Photon Nanostruct Fundam Appl* 19:12–23
12. Russell PSJ (2006) Photonic-crystal fibers. *J Lightwave Technol* 24(12):4729–4749
13. Yue Y, Kai GY, Wang Z, Sun TT, Jin L, Lu YF, Zhang CS, Liu LG, Li Y, Liu YG, Yuan SZ, Dong XY (2007) Highly birefringent elliptical-hole photonic crystal fiber with squeezed hexagonal lattice. *Opt Lett* 32:469–471
14. Sun YS, Chau YF, Yeh HH, Shen LF, Yang TJ, Tsai DP (2007) High birefringence photonic crystal fiber with a complex unit cell of asymmetric elliptical air hole cladding. *Appl Opt* 46:5276–5281
15. Sun YS, Chau YF, Yeh HH, Tsai DP (2008) Highly birefringent index-guiding photonic crystal fiber with squeezed differently sized air-holes in cladding. *Jpn J Appl Phys* 47:3755–3759
16. Chen D, Shen L (2007) Ultrahigh birefringent photonic crystal fiber with ultralow confinement loss. *IEEE Photon Technol Lett* 19:185–187
17. An L, Zheng Z, Li Z, Zhou T, Cheng J (2009) Ultrahigh birefringent photonic crystal fiber with ultralow confinement loss using four air holes in the core. *J Lightwave Technol* 27(15):3175–3180
18. Yue Y, Kai G, Wang Z, Sun T (2007) Highly birefringent elliptical-hole photonic crystal fiber with squeezed hexagonal lattice. *Opt Lett* 32(5):469–471
19. Wang L, Yang D (2007) Highly birefringent elliptical-hole rectangular lattice photonic crystal fibers with modified air holes near the core. *Opt Express* 15(14):8892–8897
20. Eguchi M, Tsuji Y (2008) Squeezed lattice elliptical-hole holey fiber. *Opt Lett* 33(16):1792–1794
21. Zhang Y-N (2010) Design and optimization of highly nonlinear low-dispersion crystal fiber with high birefringence for four-wave mixing. *Appl Opt* 49(16):3208–3214
22. Zhang Y-N (2011) Design and optimization of high-birefringence low-loss crystal fiber with two zero-dispersion wavelengths for nonlinear effects. *Appl Opt* 50(25):125–130
23. Asiful Islam M, Shah Alam M (2012) Design optimization of equiangular spiral photonic crystal fiber for large negative flat dispersion and high birefringence. *J Lightwave Technol* 30(22):3545–3551
24. Hu B, Lu M, Li W, Zou K, Zhou Z, Lin A (2010) High birefringent rhombic-hole photonic crystal fibers. *Appl Opt* 49(31):6098–6101
25. Jiang G, Fu Y, Huang Y (2015) High birefringence rectangular-hole photonic crystal fiber. *Opt Fiber Technol* 26(12):163–171
26. Karim MR, Ahmad H, Ghosh S, Rahman BMA (2018) Mid-infrared supercontinuum generation using As_2Se_3 photonic crystal fiber and the impact of higher-order dispersion parameters on its supercontinuum bandwidth. *Opt Fiber Technol* 45:255–256
27. Dudley JM, Gentyand G, Coen S (2006) Supercontinuum generation in photonic crystal fiber. *Rev Mod Phys* 78:1135–1184
28. Seddon AB (2011) A prospective for new mid-infrared medical endoscopy using chalcogenide glasses. *Int J Appl Glass Sci* 3:177–191
29. Schliesser A, Picque N, Haensch TW (2012) Mid-infrared frequency combs. *Nat Photon* 6:440–449
30. Zhao Z, Wu B, Wang X, Pan Z, Liu Z, Zhang P, Shen X, Nie Q, Dai S, Wang R (2017) Mid-infrared supercontinuum covering 2–16 μm in a low-loss telluride single-mode fiber. *Laser Photon Rev* 11:1700005
31. Wang Y, Dai S, Peng X, Zhang P, Wang X, You C (2017) Mid-infrared supercontinuum generation spanning from 1.9 to 5.7 μm in a chalcogenide fiber taper with ultra-high NA. *Infrared Phys Technol* 88:102–105
32. Eggleton BJ, Luther-Davies B, Richardson K (2011) Chalcogenide photonics. *Nat Photon* 5:141
33. Wilson RH, Tapp HS (1999) Mid-infrared spectroscopy for food analysis: Recent new applications and relevant developments in sample presentation methods. *TRAC-Trends Anal Chem* 18:85
34. Seddon AB (2011) A prospective for new mid-infrared medical endoscopy using chalcogenide glasses. *Int J Appl Glass Sci* 2:177
35. Price JHV, Feng X, Heidt AM, Brambilla G, Horak P, Poletti F, Ponzio G, Petropoulos P, Petrovich M, Shi J, Ibsen M, Loh WH, Rutt HN, Richardson DJ (2012) Supercontinuum generation in non-silica fibers. *Opt Fiber Technol* 18:327
36. Wang F, Wang K, Yao C, Jia Z, Wang S, Wu C, Qin Q, Ohishi Y, Qin W (2016) Tapered Fluro tellurite micro-structured fibers for broadband supercontinuum generation. *Opt Lett* 41:634
37. Qin G, Yan X, Kito C, Liao M, Chitrarekha C, Suzuki T, Ohishi Y (2009) Ultrabroadband supercontinuum generation from ultraviolet to 6.28 μm in a fluoride fiber. *Appl Phys Lett* 95:161–166
38. Domachuk P, Wolchover NA, Cronin-Golomb M, Wang A, George AK, Cordeiro CMB, Knight JC, Omenetto FG (2008) Over 4000 nm bandwidth of mid-IR supercontinuum generation in sub-centimeter segments of highly nonlinear tellurite PCFs. *Opt Express* 16:7161
39. Liao M, Gao W, Duan Z, Yan X, Suzuki T, Ohishi Y (2010) Supercontinuum generation in short tellurite micro-structured fibers pumped by a quasi-cw laser. *Opt Lett* 37:2127
40. Théberge F, Thiré N, Daigle J, Mathieu P, Schmidt BE, Messaddeq Y, Vallée R, Légaré F (2014) Multioctave infrared supercontinuum generation in large-core As_2S_3 fibers. *Opt Lett* 39:6474
41. Al-kadry A, Baker C, Amraoui ME, Messaddeq Y, Rochette M (2013) Broadband supercontinuum generation in As_2Se_3 chalcogenide wires by avoiding the two-photon absorption effects. *Opt Lett* 38:1185
42. Wei DP, Galstian TV, Smolnikov IV, Plotnichenko VG, Zohrabyan A (2005) Spectral broadening of femtosecond pulses in a single-mode $As-S$ glass fiber. *Opt Express* 13:2439
43. Vyas S, Tanabe T, Tiwari M, Singh G (2016) Chalcogenide photonic crystal fiber for ultra-flat mid-infrared supercontinuum generation. *Chin Opt Lett* 14:123201
44. Shiryayev VS, Churbanov MF (2013) Trends and prospects for development of chalcogenide fibers for mid-infrared transmission. *J Non-Cryst Solids* 377:225
45. An L, Zheng Z, Li Z, Zhou T (2009) Ultrahigh birefringent photonic crystal fiber with ultralow confinement loss using four air holes in the core. *J Lightwave Technol* 27(15):3175–3180
46. Huang T, Huang P, Cheng Z, Liao J, Wu X, Pan J (2018) Design and analysis of a hexagonal tellurite photonic crystal fiber with broad-band ultra-flattened dispersion in mid-IR. *Optik* 167:144–149
47. Medjouri A, Abed D, Ziane O, Simohamed LM (2018) Design and optimization of As_2S_3 chalcogenide channel waveguide

- for coherent mid-infrared supercontinuum generation. *Optik* 154:811–820
48. Aliramezani M, Mohammadnejad SH (2010) Numerical analysis and optimization of a dual-concentric-core photonic crystal fibre for broadband compensation dispersion. *Opt Laser Technol* 42:1209–1217
 49. Ehteshami N (2012) A novel broadband dispersion compensating square-lattice photonic crystal fiber. *Opt Quantum Electron* 44(6–7):323–335
 50. Hui Z, Zhang Y, Soliman A-H (2018) Mid-infrared dual-rhombic air hole $\text{Ge}_{20}\text{Sb}_{15}\text{Se}_{65}$ chalcogenide photonic crystal fiber with high birefringence and high nonlinearity. *Ceram Int* 44:10383–10392
 51. Li X, Liu X, Hu X (2010) Long-cavity passively mode-locked fiber ring laser with high-energy rectangular-shape pulses in anomalous dispersion regime. *Opt Lett* 35(19):3249–3251
 52. Zhang H, Tang DY, Zhao LM (2010) Compact graphene mode-locked wavelength-tunable erbium-doped fiber lasers: from all anomalous dispersion to all normal dispersion. *Laser Phys Lett* 7(8):591–596
 53. Saghaei H (2017) Supercontinuum source for dense wavelength division multiplexing in square photonic crystal fiber via fluidic infiltration approach. *Radioengineering* 26(1):16–22
 54. Valliammai M, Sivabalan S (2017) Wideband supercontinuum generation in mid-IR using polarization maintaining chalcogenide photonic quasi-crystal fiber. *Appl Opt* 56:4797–4806

Publisher's Note Springer Nature remains neutral with regard to jurisdictional claims in published maps and institutional affiliations.